ROPOD: Force Sensorless Compliant Control for Mobile Robots

J.J.E. Unkel

CST 2018.037

Master's thesis

Coach: Dr. C.A. Lopez Martinez MSc.

Supervisors: Prof. Dr. H.P.J. Bruyninckx
Dr. Ir. M.J.G. van de Molengraft

Committee: Prof. Dr. H.P.J. Bruyninckx
Dr. Ir. R.H. Cuijpers
Dr. Ir. M.J.G. van de Molengraft

Eindhoven University of Technology
Department of Mechanical Engineering
Control Systems Technology

Eindhoven, March 21, 2018

CONTENTS

ROPOD: Force Sensorless Compliant Control for Mobile Robots

J.J.E. Unkel, C.A. Lopez, M.J.G. van de Molengraft, H.P.J. Bruyninckx

***Abstract*—Automated guided vehicles (AGVs) are quickly gaining popularity for logistic purposes in industrial environments and the trend now is to also employ them in environments shared with people. These vehicles are capable of autonomously transporting goods in for example warehouses and factories. A limitation of most currently existing AGVs is that they do not allow physical interaction with people, meaning they either have to operate in controlled environments or are likely to disrupt people in an inconvenient way which is difficult to correct. In this research a control strategy that allows an AGV to safely interact with people in a compliant way without the use of additional force sensors is developed. This is an important feature with regards to safety, such that people can push the AGV with its load out of the way when desired, especially in an emergency situation. This sensorless compliant control is achieved with the combination of a disturbance observer with impedance control. The AGV has to be able to transport loads with large differences in mass, so a method has been developed which is capable of quickly estimating this mass with the aim to preserve performance and stability. Design guidelines are given on how to select the compliant parameters. Several safety features have been implemented, such as a velocity and acceleration limit in order to reduce the risk of damage in case of a collision. Experimental results are shown in which the proposed methods are successfully verified on a mobile robot.**

***Index Terms*—Compliant control, Disturbance observer, Mobile robot.**

I. Introduction

The transportation of goods and carts in small logistic tasks is often executed by humans. Think of for example trolleys, carts and sick beds in a hospital. This not only prevents these people from doing more important work, but can also cause physical strain and potentially injuries when carrying large and heavy loads. A potential alternative would be the use of automatically guided vehicles (AGVs). AGVs exist already since 1950 and their use have been growing ever since [1]. These AGVs will carry the load to their destination, relieving employees from physical strain and allowing them to work on other tasks in the mean time.

Even though the potential of AGVs is huge and their market is growing, their success is relatively low compared to other industrial robots. A few possible explanations for this lack of success are:

- The AGVs usually have to operate in the same environment as humans, meaning that there are significant risks of collisions and injuries if the AGV cannot safely interact with them.
- The tasks which have to be performed by these AGVs are often not repetitive, but highly dependent on which object they have to carry and to which destination. Also the environment in which these AGVs have to operate is not fully known.
- There are dozens of different loads that need to be carried, all with different sizes, shapes and connection mechanisms. There is not one standard which is being used.
- Lastly, the current available AGVs are rarely flexible and scalable. This means the AGVs are fit for only one specific task and if a company's task differs slightly, a large reconfiguration effort is needed to use the AGV.

This is where the robotic pod (ROPOD)[1] project comes into play [2]. The ROPOD project is a collaboration between the '*Katholieke Universiteit Leuven*', '*Technische Universiteit Eindhoven*', '*Agaplesion Frankfurter Diakonie Kliniken Gemeinnutzige Gmbh*', '*Speciaal Machinefabriek Ketels Vof*', '*Locomotec Gmbh*' and '*Bonn-Rhein-Sieg University of Applied Sciences*'.

The goal of this collaboration project is to overcome the previously mentioned shortcomings of current AGVs and to create Automated Guided Vehicles which are low-cost, small and can be implemented without expensive modifications to the buildings they are used in. These robotic pods (ropods) should be able to move different types of payloads without the need of modifying existing trollies, carts etc. For larger loads such as hospital beds, the ropods should be able to cooperate and move in flocks to move loads which they normally would not be able to carry alone. The ropods will work in a partially known environment and have the capability to plan their own route throughout the building. The ropods will operate in an environment where people are present, so to ensure safe interaction and avoid the ropods of getting in the way, the ropods should offer compliant control and should move as close as possible to walls to limit the chance of collision. Force sensors on the ropod will be used for compliant control during normal operation. The ropod is designed to feature holonomic movements due to passive safety, meaning that it does not get stuck in any direction when not powered.
The compliant control allows people to move the ropod around without requiring large amounts of force. This will allow people to move the ropods easily when they obstruct the way. Moreover, it is highly desirable to have compliant behavior even when people do not interact via the force

[1]In this work, when referring to the robotic pod project, ROPOD is used. When referring to a robotic pod itself, ropod is used.

sensors. This is important with regards to safety is in an emergency situation. When there is an emergency, people should be able to interact with the ropod even when they do not use the force sensors attached to the robot. Hospital staff could be trained to work with the ropod and the force sensors, but this can be easily forgotten during an emergency. Also visitors of the hospital who have never worked with a ropod before should be able to interact with the ropod in a safe and compliant way. In some scenarios it is even nearly impossible to reach for the force sensors, for example when it is carrying a large load above itself. The goal of this project is therefore to achieve compliant behavior for a wheeled mobile robot, without the use of any force/torque sensing sensors.

Work has already been done in the area of compliant control for robotics. A common application for compliant control is in the field of humanoid robots. Here it allows robots to safely interact with objects [3] [4] or humans [5], however force/torque sensors are used. Compliant control for wheeled mobile robots has been done before as well, for example in [6] [7] [8]. Again, in this work, a force/torque sensor is used to get an estimate of the applied forces. Sensorless force control has been studied before in [9] where a disturbance observer is used to detect collisions with people and react accordingly. Force control without force sensors has been investigated in [10] where fault detection and isolation is used to detect a collision on a robotic arm. After a collision, the control switches to interaction force control to maintain a safe interaction. In [11] a disturbance observer is used in an exoskeleton. This exoskeleton aids a user with certain tasks via compliant control. Very relevant research has been done in [12], where a compliant wheelchair is developed. Here, force sensors are used for the human input, while a disturbance observer estimates the environmental forces on the wheelchair. These inputs are used to achieve compliant behavior via impedance control. These previously mentioned papers all assume that the system is known beforehand and that it does not change. This research is based on [9] and [12] but with the addition of trying to maintain performance and stability for varying masses and to present design guidelines and indications of stability and performance.

This research is split up in the following Sections. In Section II the problem statement is given along with the objectives belonging to this problem statement. A dynamic model of the robots used is given in Section III. In Section IV several compliant controllers will be discussed and three will be developed in further detail. In Section V a disturbance observer is presented which is combined with the compliant control in Section VI. Next a method to quickly identify the robots parameters is discussed in Section VII and the compliant control is experimentally verified in Section VIII. In Section IX several safety features are discussed and finally in Section X conclusions will be drawn and recommendations for future work are given.

II. Problem Statement

The goal of this research is to allow the ropod to offer compliant control without using force sensors for varying loads of different dimensions and weights through a hospital. These loads are currently existing carts and trolleys, so the ropod should be capable of handling this variety and thus it should adapt accordingly. For this research, the compliant control does not take into account additional kinematic constraints imposed by the load. The ropods will operate in an area which is also used by humans at the same time. This means the ropod will have to be able to interact with people and the environment in a compliant way.

A. Objectives

The following objectives can be drawn from the problem statement:

- *Offer compliant control with humans and the environment without the use of force sensors.*
  There are several types of configurations of ropod and load possible and in different scenarios, however in this research the compliant control will be developed for the ropod without carrying a load. The ropod should be compliant in the sense that users can easily rotate and translate the ropod if necessary.
- *Be able to handle large variations in dynamics.*
  The ropod should be able to handle different objects, all with different masses while still being stable and able to react in a compliant way.

B. Requirements

There are several requirements which restrict the potential solutions.

- *Stability against mass variations*
  The lowest expected mass is the mass of the ropod itself, while the highest expected mass can be up to 500kg of a hospital bed with patient.
- *Limit actuation force*
  Each motor of the ropod will be rated for a maximum continuous power draw. To ensure the lifespan of the motors, the maximum power output should not exceed their maximum rating.
- *Help to a maximum velocity*
  The average preferred walking speed of humans is around 5 km/h or 1.4 m/s [13]. This means the maximum velocity to which the ropod will help the user will also be 5 km/h or 1.4 m/s. At velocities higher than this limit, the ropod will only offer reduced amounts of aid.
- *Limit the maximum acceleration caused by the compliant control*
  To maintain a smooth ride for the ropod and its load, the compliant control will only aid in accelerating up to a certain limit. If a user wants to accelerate faster than this limit, then this is still possible, however they have to provide this force on their own.

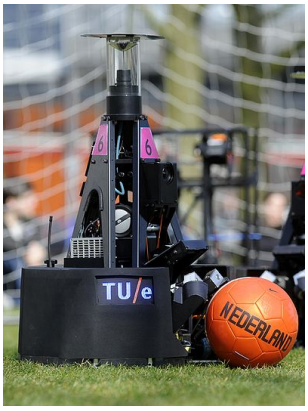

(a) Photograph of the TURTLE soccer robot

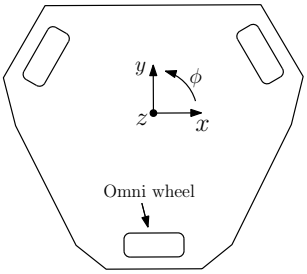

(b) Top-down view drawing of the base of the TURTLE with axes

Fig. 1: Soccer robot of Tech United

III. Dynamical System

Initially the aim was to use a ropod for this research project. However this was not available and thus a different holonomic robot has been used. This robot is the Tech United soccer robot called TURTLE which is a robotic platform which uses three omni-directional wheels in a triangular layout to achieve holonomic movements. A picture and schematic drawing of this robot and its degrees of freedom are shown in Figure 1.

The three axes are two translational axes x and y and the rotational axis ϕ. This robot has been modeled as three independent mass damper systems with coulomb friction given by the following Equation

$$M_{\text{n}}\ddot{x} + D_{\text{n}}\dot{x} + F_{\text{fric,n}} = F + F_{\text{dist}}, \tag{1}$$

with $M_{\text{n}}, D_{\text{n}}$ and $F_{\text{fric,n}}$ represent the system's mass, damping and coulomb friction respectively. For the translational axes the state x is defined as the position of the robot in meters while for the rotational axis the state is defined as the angle of the robot in radians. The subscript $*_{\text{n}}$ indicates that the parameters are the nominal system parameters. The control input is given by F and the external disturbance force is given by F_{dist}. The values of the mass, damping and coulomb friction together with their 95% confidence bounds are given in Table I. More detail on the model and parameter estimation is shown in Appendix A.

IV. Compliant Control

Compliant behavior can be realized in several ways. The main concepts and their advantages and disadvantages will be discussed in this Section.

Axis	Mass	Viscous damping	Coulomb friction
x	36.5 kg	1.852 ± 0.473 Ns/m	26.870 ± 0.5640 N
y	36.5 kg	1.126 ± 0.378 Ns/m	26.167 ± 0.430 N
ϕ	0.73 ± 0.06 kgm^2	0.119 ± 0.024 Ns	4.686 ± 0.073 Nm

TABLE I: Identified parameters of the system

A. Indirect Compliance

One of the simpler forms of compliance is indirect compliance. Indirect compliance is compliance where no direct or estimated force measurements are used in the control scheme [14]. If the designed control scheme only uses a proportional gain, the reaction force exerted on the environment is proportional to the control error. The downside of indirect compliance with respect to the ROPOD project is that it does not allow users to push the ropod out of the way with a small amount of force. Instead, it acts like there is a physical spring attached between the ropod and the reference point. Moreover there is no active support to reduce apparent mass and damping.

B. Direct Compliance

With direct compliance, the input of force sensors, or in this case the disturbance estimate from the disturbance observer from Section V is used. The control algorithm uses this control input to determine how the robot should react such that its behavior is compliant. Applying direct compliant control to omni-directional robots has been studied before, for example in [6]. In this papers, compliant control has been applied to an omni-directional robot. For the compliance, admittance control in combination with torque sensors to measure the applied force have been used. Another frequently used direct compliance technique is impedance control, which is very similar to admittance control as discussed in [15]. Impedance control is often used in achieving compliant behavior in robots such in [8] and [16]. However, in all this research force/torque sensors are used. Impedance control without the use of force sensors has been used in [12]. For the force of the user, a force sensor is used, however for disturbances coming from the environment the disturbance observer is used. Both force estimates are then used for impedance control which helps the user push a wheelchair. Another compliant method is discussed in [7] where force feedback is used to achieve compliance. Here, torque sensors are used to measure the interaction force and a feedback controller then tries to control this force to zero. These three compliant control strategies, impedance control, admittance control and force feedback control will be investigated in further detail.

C. Impedance Control

The first direct compliant algorithm is impedance control. With impedance control the robot responds to movements by generating control input. The relationship between movement and forces can be chosen in such a way that the system will 'feel' like a different system with different properties. For example, the 'virtual' mass can be chosen lower than the real mass of the system. This way the user will have to exert less force in order to accelerate the system. In the same way the 'virtual' friction can be lowered, resulting in less force required to keep the robot moving at a constant velocity. A block diagram of this control scheme is shown in Figure 2.

In this Figure, x_{ref} is a chosen reference trajectory that the system should follow, x is the position of the robot, F is the control input to the system and F_{ext} is the external disturbance

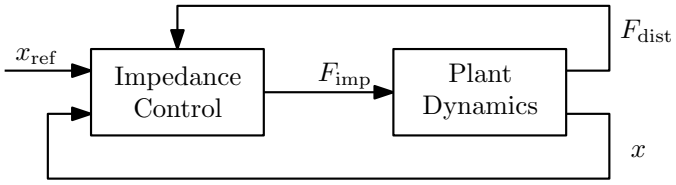

Fig. 2: Block diagram of impedance control

force.

Recall the equations of motion defined in (1). The goal of impedance control is to change the input-output behavior of the system to match the following desired system

$$M_{\text{d}}\ddot{e} + D_{\text{d}}\dot{e} + F_{\text{fric,d}} = F_{\text{dist}}, \tag{2}$$

where $e = x - x_{\text{ref}}$, the error between the reference trajectory and the systems position and the subscript $*_{\text{d}}$ indicates that the parameters are the desired parameters. Equation (1) can be rewritten as

$$F = M_{\text{r}}\ddot{x} + D_{\text{r}}\dot{x} - F_{\text{dist}} + F_{\text{fric,r}}. \tag{3}$$

Substituting (2) into (3) results in

$$\begin{aligned} F = (M_{\text{n}} - M_{\text{d}})\ddot{x} + (D_{\text{n}} - D_{\text{d}})\dot{x} + M_{\text{d}}\ddot{x}_{\text{ref}} + D_{\text{d}}\dot{x}_{\text{ref}} \\ - F_{\text{fric,d}} + F_{\text{fric,n}}, \end{aligned} \tag{4}$$

where $\ddot{x}$ can be replaced by rewriting equation (1) resulting in the following expression

$$\begin{aligned} F = \left(\frac{M_{\text{n}}}{M_{\text{d}}} - 1\right) F_{\text{dist}} + \frac{D_{\text{d}}M_{\text{n}}}{M_{\text{d}}}\dot{x}_{\text{ref}} + M_{\text{n}}\ddot{x}_{\text{ref}} \\ + \left(D_{\text{n}} - \frac{D_{\text{d}}M_{\text{n}}}{M_{\text{d}}}\right)\dot{x} + F_{\text{fric,n}} - \frac{M_{\text{n}}}{M_{\text{d}}}F_{\text{fric,d}} \end{aligned} \tag{5}$$

which ensures that the system will behave as described in Equation (2).

D. Admittance Control

The second compliant control strategy is admittance control. Admittance control tries to achieve the same desired dynamical system as described in (2). However, it does this with the use of an inner position controller and an outer admittance controller. The admittance controller generates a reference trajectory based on the desired plant dynamics, the reference x_{ref} and measured disturbance force and feeds this trajectory to the inner position controller. A schematic overview can be found in Figure 3.

The internal position controller can be any kind of stabilizing controller, but the bandwidth and properties of the controller have impact on total compliant performance. The

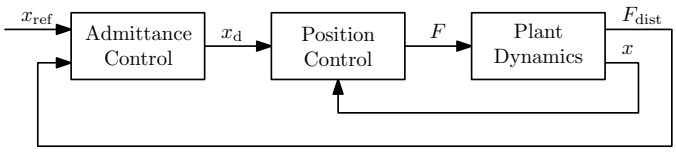

Fig. 3: Block diagram of admittance control

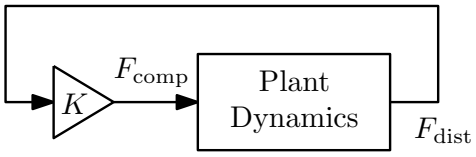

Fig. 4: Block diagram of Force Feedback

reference trajectory is generated by the following desired system dynamics:

$$M_{\text{d}}(\ddot{x}_{\text{d}} - \ddot{x}_{\text{ref}}) + D_{\text{d}}(\dot{x}_{\text{d}} - \dot{x}_{\text{ref}}) + F_{\text{fric,d}} = F_{\text{dist}}. \tag{6}$$

This will result in the desired compliant dynamics described in (2), but only in the region of the bandwidth of the position controller.

E. Force Feedback

The third and more simpler approach is to assist the user by magnifying their own input force with a certain gain K and helping with that amount. A schematic overview of this is given in Figure 4.

The main advantage of this method is the small amount of tunable parameters compared to the previous two methods. There is only a magnification gain. However this is also a disadvantage at the same time, since all applied forces get magnified, resulting in a decrease in sensed mass, damping and friction simultaneously, thus there is no possibility of changing individual parameters.

V. Disturbance Observer

For the previously discussed active compliant control strategies, the disturbance force is required to be known. Since this research is focused on force sensorless compliant control, a method has to be developed which estimates the users forces. A commonly used method to estimate external disturbance forces is with the use of a disturbance observer [17] [18]. The basic control scheme of a disturbance observer is shown in Figure 5.

In this Figure, F^{in} represents a certain input force to the system, F^{dist} is a disturbance force acting on the system, which can be a user interacting with the robot, x is the position of the system and $\hat{F}^{dist}$ is the estimation of F^{dist}. The models

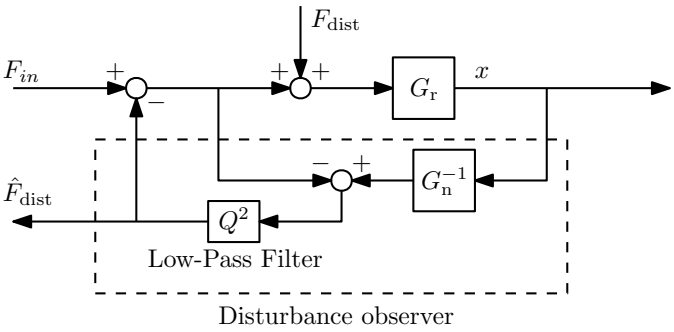

Fig. 5: Block diagram of a disturbance observer

G_r and G_n represent the real system and the nominal model of the real system respectively. Since the inverse of G_n can be non-causal and to prevent an algebraic loop, the low-pass filter Q is required. The low-pass filter also reduces high frequent measurement noise and determines the bandwidth of the disturbance observer. The disturbance observer uses the position of the system as its input, meaning that it can only observe forces if the system is in motion. This has the effect that the user has to overcome the static friction of the system themselves before the observer is capable of estimating their force.

A. Input Output Behavior

Based on the block diagram in Figure 5 it is possible to write down the transfer functions of the disturbance observer. The input-output transfer functions of the disturbance observer are as following

$$x(s) = G^o_{F^{in}x}(s)F_\mathrm{in}(s) + G^o_{F_\mathrm{dist}x}F_\mathrm{dist}(s), \tag{7}$$

where:

$$\begin{aligned} G^o_{F^{in}x} &= \frac{G_\mathrm{r}G_n}{G_\mathrm{n} + (G_\mathrm{r} - G_\mathrm{n})Q} \\ G^o_{F^{dist}x} &= \frac{G_\mathrm{r}G_\mathrm{n}(1-Q)}{G_\mathrm{n} + (G_\mathrm{r} - G_\mathrm{n})Q}. \end{aligned} \tag{8}$$

In the frequency domain where $Q(s) \approx 1$, meaning inside the bandwidth of the disturbance observer, the transfer functions reduce to:

$$\begin{aligned} G^o_{F^{in}x} &\approx G_\mathrm{n} \\ G^o_{F^{dist}x} &\approx 0, \end{aligned} \tag{9}$$

resulting in the system behaving as the nominal model G_n, also called nominal model following and rejecting disturbances. In the region where $Q(s) \approx 0$ the system behaves as:

$$\begin{aligned} G^o_{F^{in}x} &\approx G_\mathrm{r} \\ G^o_{F^{dist}x} &\approx G_\mathrm{r}, \end{aligned} \tag{10}$$

meaning the system will behave as the original system and disturbances will no longer be rejected. This has the same effect as not having the disturbance observer altogether.

B. Disturbance Estimation

The main use of the disturbance observer is not the nominal model following or disturbance rejection, but the disturbance estimation. This estimate can later be used for the compliant control. The disturbance estimate $\hat{F}_\mathrm{dist}$ has the following transfer function

$$\begin{aligned} \hat{F}_\mathrm{dist}(s) = &\frac{Q(G_\mathrm{r} - G_\mathrm{n})}{G_\mathrm{n} + (G_\mathrm{r} - G_\mathrm{n})Q}F_\mathrm{in}(s) \\ &+ \frac{G_\mathrm{r}Q}{G_\mathrm{n} + (G_\mathrm{r} - G_\mathrm{n})Q}F_\mathrm{dist}(s). \end{aligned} \tag{11}$$

In the scenario where $Q(s) \approx 1$ and $G_\mathrm{n} = G_\mathrm{r}$ then

$$\hat{F}_\mathrm{dist}(s) \approx F_\mathrm{dist}(s), \tag{12}$$

indicating that the disturbance F_dist is estimated by $\hat{F}_\mathrm{dist}$. In practice though, G_n will never be exactly equal to G_r. The difference between the real system and the nominal model has an impact on the accuracy of the disturbance estimation. In other words, in the case that $Q(s) \approx 1$ and $G_\mathrm{n} \neq G$ the transfer function becomes

$$\hat{F}_\mathrm{dist}(s) \approx \frac{G_\mathrm{r} - G_\mathrm{n}}{G_\mathrm{r}}F_\mathrm{in}(s) + F_\mathrm{dist}(s). \tag{13}$$

This shows that when the nominal model G_n does not exactly match the real system G the estimated disturbance $\hat{F}_\mathrm{dist}$ is no longer a perfect estimate of F_dist. This means that when combining the disturbance observer with the compliant control, stability and performance are not immediately guaranteed. The stability and performance of this combination will be discussed in further detail in Section VI.

In Section IV a form of compliant control is discussed for which a small change in the disturbance observer is required. Impedance control uses the velocity of the system $\dot{x}$ and the disturbance force F_dist. However if we recall Equation (9), under ideal conditions, disturbances will be rejected by the disturbance observer. This means the system will not move freely under the effects of external disturbances, however for the impedance control, it is essential for the system to respond to the disturbances. This problem can be solved by removing the feedback loop shown in Figure 5. This does have an impact on the disturbance estimation. The disturbance estimation for the new situation is given as following

$$\hat{F}_\mathrm{dist}(s) = \frac{Q(G_\mathrm{r} - G_\mathrm{n})}{G_\mathrm{n}}F_\mathrm{in}(s) + \frac{G_\mathrm{r}Q}{G_\mathrm{n}}F_\mathrm{dist}. \tag{14}$$

Again in the scenario where $Q(s) \approx 1$ and $G_\mathrm{n} = G_\mathrm{r}$ then the transfer-function reduces to

$$\hat{F}_\mathrm{dist}(s) \approx F_\mathrm{dist}(s), \tag{15}$$

which means that $\hat{F}_\mathrm{dist}$ is still perfectly estimating F_dist. Things do change when the nominal model G_n is no longer equal to G_r while $Q \approx 1$. The disturbance estimation then is described as

$$\hat{F}_\mathrm{dist}(s) \approx \frac{G_\mathrm{r} - G_\mathrm{n}}{G_\mathrm{n}}F_\mathrm{in} + \frac{G_\mathrm{r}}{G_\mathrm{n}}F_\mathrm{dist}. \tag{16}$$

This shows that there is a difference in the disturbance estimation between the two versions. The consequences of this in combination with compliant control will be investigated in Section VI.

VI. Combining Observer with Compliant Control

After the disturbance observer and compliant control have been separately analyzed, it is possible to combine the disturbance observer with the compliant control. The output of the observer can be used as an input of the compliant control. Initially for the stability analysis the friction of the nominal system as well as the friction of the desired system is omitted such that linear theory can be applied. The stability of the system with friction is presented in Appendix B. Furthermore the reference input x_ref is removed as the goal of this project is

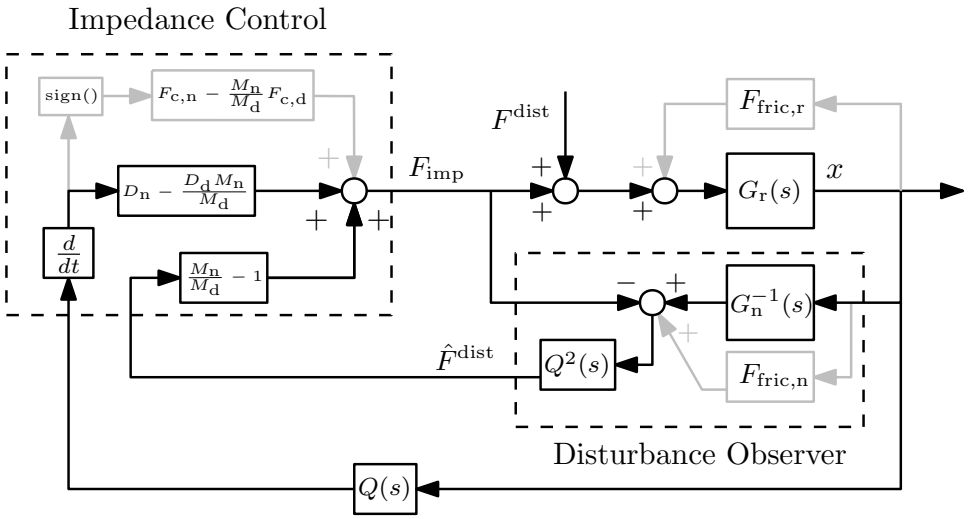

Fig. 6: Disturbance observer combined with impedance control. The blocks in black represent the linear dynamics while the blocks in gray represent the non-linear friction dynamics.

to respond compliantly to disturbance forces and not to follow a trajectory. The stability criteria presented in this Section are under the assumption $Q(s) \approx 1$, meaning they are design guidelines for tuning the parameters and cannot guarantee absolute stability. From now on this will be referred to as an ideal system. To check the stability of the systems without this assumption, the closed-loop poles can be computed numerically using specific values for all the parameters.

A. Stability Analysis - Impedance

The combination of impedance control with disturbance observer is shown in Figure 6. The gray blocks represent the non-linear friction terms, which are for now omitted. The stability with these blocks included is discussed in Appendix B. In Figure 6, the impedance control is represented by Equation (5) and the disturbance observer as discussed in Section V. For a system to be stable, the closed-loop input-output transfer-function should have all poles in the open left half plane. The input-output closed-loop transfer-function of the system is given by

$$\frac{x}{F_{\text{dist}}} = \frac{G_\mathrm{r} G_n \left(\left(\frac{M_\mathrm{n}}{M_\mathrm{d}} - 1 \right) Q^2 + 1 \right)}{G_n + Q^2 \left(G_n - G_\mathrm{r} \right) \left(\frac{M_\mathrm{n}}{M_\mathrm{d}} - 1 \right) - G_\mathrm{r} G_n Q \left(D_\mathrm{n} - \frac{D_\mathrm{d} M_\mathrm{n}}{M_\mathrm{d}} \right) s} \tag{17}$$

with the sub transfer-functions defined as following:

$$\begin{aligned} G_\mathrm{r}(s) &= \frac{1}{M_\mathrm{r} s^2 + D_\mathrm{r} s} \\ G_n(s) &= \frac{1}{M_\mathrm{n} s^2 + D_\mathrm{n} s} \\ Q(s) &= \frac{g_{dis}}{s + g_{dis}}. \end{aligned} \tag{18}$$

Under the assumption that $Q(s) \approx 1$, the closed-loop transfer-function of the ideal system is equal to

$$G_{\text{imp,ideal}} = \frac{1}{\left(M_\mathrm{r} - M_\mathrm{n} + M_\mathrm{d} \right) s^2 + \left(D_\mathrm{r} - D_\mathrm{n} + D_\mathrm{d} \right) s}. \tag{19}$$

This shows that if the nominal parameters are not equal to the real parameters, the sensed mass and/or damping by the user are no longer equal to the desired values The poles of (19) are:

$$\begin{aligned} s &= 0 \\ s &= -\frac{D_\mathrm{r} - D_\mathrm{n} + D_\mathrm{d}}{M_\mathrm{r} - M_\mathrm{n} + M_\mathrm{d}}. \end{aligned} \tag{20}$$

Generally a system is considered to be stable if all poles lie in the open left half plane, meaning no poles at $s = 0$. In this case the pole at $s = 0$ is caused by the fact that there is no stiffness in the system, but that is intentional so the pole at $s = 0$ is not a problem. The other poles are in the negative left half plane if: $D_\mathrm{r} - D_\mathrm{n} + D_\mathrm{d} > 0$ and $M_\mathrm{r} - M_\mathrm{n} + M_\mathrm{d} > 0$. The combination of both terms being negative is not possible. For more detail about this see Appendix B. A conservative approach is that, assuming all parameters are positive, if the nominal parameters are smaller than the real system parameters the system is stable. In the frequency region where $Q(s) \approx 0$, (17) reduces to

$$G_{\text{imp,Q=0}} = \frac{1}{M_\mathrm{r} s^2 + D_\mathrm{r} s} \tag{21}$$

which is the original system without any compliant control.

B. Stability Analysis - Admittance

The combined control scheme of admittance control with disturbance observer is shown in Figure 7. The admittance controller is defined by (6) and the position controller can be any stable controller. This control scheme can be expanded in a similar fashion as Figure 6. The input-output transfer-function is given by

$$\frac{x}{F_{\text{dist}}} = \frac{G_\mathrm{r} G_\mathrm{n} \left(1 - Q^2 + C_\mathrm{p} G_\mathrm{d} Q^2 \right)}{\left(G_\mathrm{r} - G_\mathrm{n} - C_\mathrm{p} G_\mathrm{r} G_\mathrm{d} + C_\mathrm{p} G_\mathrm{d} G_\mathrm{n} \right) Q^2 + G_\mathrm{n} + C_\mathrm{p} G_\mathrm{r} G_\mathrm{n}} \tag{22}$$

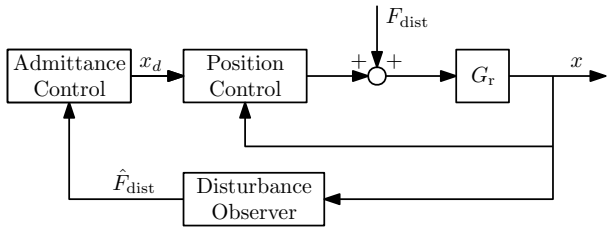

Fig. 7: Disturbance observer combined with admittance control

with $G_{\text{r}}, G_{\text{n}}, Q$ defined in (18) and G_{d} defined as

$$G_{\text{d}}(s) = \frac{1}{M_{\text{d}}s^2 + D_{\text{d}}s}. \tag{23}$$

Again for the ideal system where $Q(s) \approx 1$ and under the assumption of a perfect position controller, the closed-loop transfer-function is equal to (19) and with poles equal to (20) which results in the same stability criteria as for the impedance control. In the frequency region where $Q(s) \approx 0$ the transfer-function becomes

$$G_{\text{adm,Q=0}} = 0. \tag{24}$$

This is caused by the fact that the output of the disturbance observer in this region is equal to 0, meaning no reference trajectory will be generated and thus the robot will not move.

C. Stability Analysis - Force Feedback

The combined control scheme of the force feedback with disturbance observer is shown in Figure 8. The closed-loop transfer-function of this system is given by

$$\frac{x}{F_{\text{dist}}} = \frac{G_{\text{r}}\left(KG_{\text{n}}Q^2 + G_{\text{n}}\right)}{G_{\text{n}} - KG_{\text{r}}Q^2 + KG_{\text{n}}Q^2}. \tag{25}$$

In the ideal situation where $Q(s) \approx 1$ the closed-loop transfer-function can be written as

$$G_{\text{ff,ideal}} = \frac{K+1}{\left(M_{\text{r}} - KM_{\text{n}} + KM_{\text{r}}\right)s^2 + \left(D_{\text{r}} - KD_{\text{n}} + KD_{\text{r}}\right)s} \tag{26}$$

which has poles at:

$$\begin{aligned} s &= 0 \\ s &= -\frac{\left(D_{\text{r}} - D_{\text{n}}\right)K + D_{\text{r}}}{\left(M_{\text{r}} - M_{\text{n}}\right)K + M_{\text{r}}}. \end{aligned} \tag{27}$$

This results in a stable system if $\left(D_{\text{r}} - D_{\text{n}}\right)K + D_{\text{r}} > 0$ and $\left(M_{\text{n}} - M_{\text{r}}\right)K - M_{\text{r}} > 0$. Again, the combination of both terms being negative is not possible for reasons explained in Appendix B. A conservative stability criteria is again that if the nominal parameters are smaller or equal to the real parameters, the system will be stable. In the region where $Q(s) \approx 0$ the transfer-function is equal to (21).

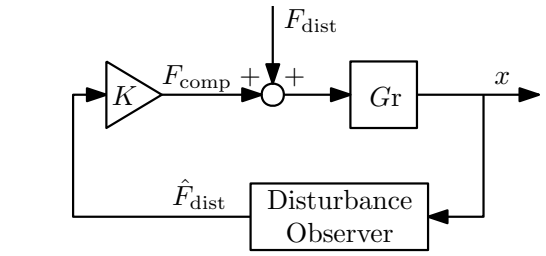

Fig. 8: Disturbance observer combined with Force Feedback

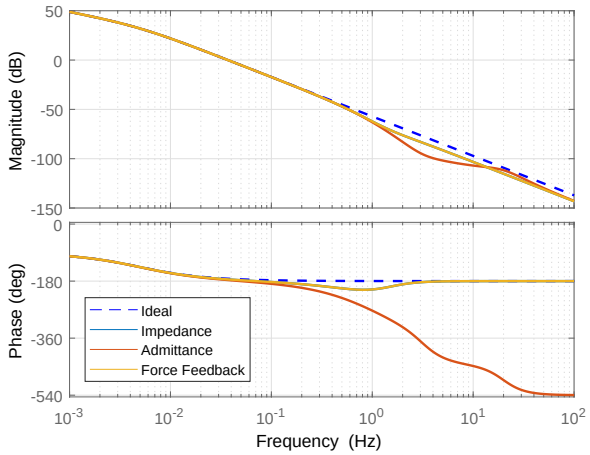

Fig. 9: Bode plots of the different compliant control algorithms

D. Performance Comparison

To visualize the differences between the three discussed algorithms, bode plots of the y-direction are shown in Figure 9. The 'real' parameters M_{r} and D_{r} are taken from Table I. This scenario considers the situation where the nominal parameters M_{n} and D_{n} are equal to the 'real' parameters M_{r} and D_{r} respectively. The force gain K is set to 1, so for a fair comparison, M_{d} and D_{d} are chosen as half of the nominal parameters. The position controller for admittance control is chosen as a lead-lag filter with pole and zero at 0.01 Hz and 20 Hz respectively and a gain of 300. This results in a bandwidth of 16.2 Hz.

As can be seen from Figure 9, the performance of all three compliant control algorithms at low frequencies are identical and equal to the desired performance. At higher frequencies, all three compliant control algorithms start to deviate from the desired system.

Both impedance control and force feedback control show a transition from the desired performance to the nominal performance. Admittance control however dips below nominal performance, meaning that the robot will feel heavier to a user than it actually is. This effect is caused by the difference in bandwidth of the disturbance observer and the internal position controller. At input frequencies above the bandwidth of the observer, hardly any forces will be observed. Meaning a reference trajectory of zero will be generated. The position controller will then actively try to follow this reference resulting in the controller opposing the users input. Another comparison is made for the situation where M_{n} and D_{n} are $0.75M_{\text{r}}$ and $0.75D_{\text{r}}$ respectively. The bode plots of this are shown in Figure 10.

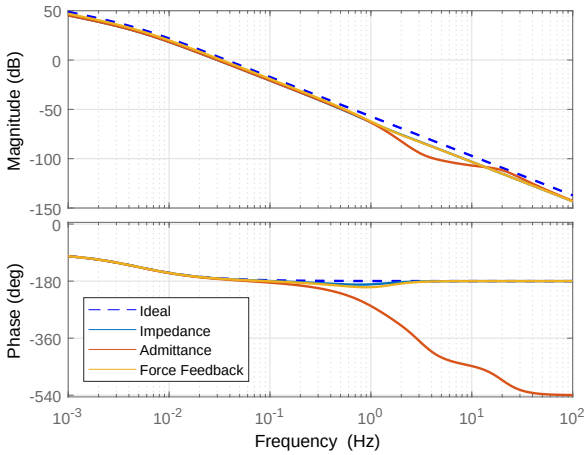

Fig. 10: Bode plots of the different compliant control algorithms

These Figures show that the performance at low frequencies is no longer identical to the desired performance. This is caused by the difference in the 'real' and nominal parameters as shown in (19) for impedance and admittance control and in (26) for the force-feedback control.

E. Compliant Control Selection

At this point, a choice has to be made between the three compliant control algorithms who all try to achieve the same desired dynamical properties. The main difference between admittance and impedance control lies in the fact that admittance control uses a position controller while impedance control uses the nominal system parameters. However, the compliant control will be used in combination with a disturbance observer which uses the the nominal parameters. This means that when using admittance control the nominal parameters are still required to be known. So for this research project, admittance control depends on the same parameters as impedance control, but also uses a position controller. Since the compliant control has to be able to cope with large parameter variations, the performance of the position controller can also change significantly and thus in turn the performance of the compliant control can change significantly. Lastly in the region between the bandwidths of the disturbance observer and the position controller, the robot will actually feel heavier to the user than the original system without control. The force feedback method is relatively simple since it only has one tuning parameter K, however the same performance can be achieved with impedance and admittance control while allowing for more freedom in dynamics. So taking into account simplicity, stability and freedom in dynamics, impedance control has been chosen to be used for experimental validation.

VII. Parameter Identification

As shown in Section VI, the performance and stability of the combined system heavily depends on the accuracy of the nominal parameters. Since the ropod has to deal with large variations in loads, a method to quickly identify the new parameters is desired. For stability reasons discussed previously, the estimated parameters should always be smaller or equal to the 'real' parameters.

A. Identification Methods

One method to estimate system parameters is using iterative feed-forward tuning [19]. This method aims to estimate the systems parameters in order to improve feed-forward. These estimated parameters can also be used as the nominal system parameters. However this method is not capable of dealing with static/coulomb friction and can thus overestimate the parameters, which can compromise the stability of the system. Another method which does take friction into account is presented in [20]. This method is capable of estimating coulomb friction, but uses many different measurements at different velocities to achieve this. The required method though has to be able to estimate the new parameters quickly while using a limited amount of space. Also the procedure has to be relatively smooth in order to not disturb the load too much, meaning frequency response measurements over a large range of frequencies is also not an option. Based on these requirements the chosen method involves making small sinusoidal movements to estimate the parameters. The parameters to be estimated are the mass, viscous damping, static friction and coulomb friction. However, if the friction can be modeled as shown in Figure 17, then the viscous damping and coulomb friction are nearly impossible to identify at low velocities. So for this identification, the viscous damping and the coulomb friction are neglected and only the static friction and mass/inertia will be estimated. The viscous damping and coulomb friction determined previously will be used again after the identification. The developed identification procedure is as following:

- *Determine static friction*
  First the static friction of the system will be estimated by slowly increasing the input force until the robot starts to move. This experiment will be repeated several times to get the maximum static friction.
- *Apply a sinusoidal input force with static friction feed-forward*
  A sine wave with a frequency which will mostly excite the mass dynamics of the system is applied to the robot. To compensate for the friction present, a feed-forward signal is added such that ideally only the mass dynamics remain present.
- *Determine mass from measured acceleration*
  To determine the mass/inertia of the system a Fast Fourier transformation is taken from the measured acceleration. The magnitude of the input sine wave is then divided by the magnitude of the measured acceleration at the same frequency of the input sine wave resulting in the estimated mass/inertia.

The result is an estimated mass/inertia which is always equal to or smaller than the real mass/inertia. This is achieved because,

Experiment	Estimated mass (kg)	Estimated inertia (kgm^2)
1	31.41	0.579
2	30.63	0.591
3	30.68	0.564
4	31.65	0.581

TABLE II: Estimated mass and inertia of the unmodified robot. Mass and inertia are estimated in separate experiments

for low velocities, the friction compensation will always be larger than the real effective friction on the system as can be seen from Figure 17. Since the friction compensation will be too large, the measured acceleration will be larger than if the friction would be perfectly compensated for and thus the estimated mass/inertia will be lower than the actual mass/inertia. After the parameter estimation, the new parameters will be used for the compliant control. For the viscous damping and coulomb friction, the initial values of the robot without load will be used. This will not cause any stability issues since it is assumed that both viscous damping and coulomb friction will only increase if the mass of the robot-load combination increases. For performance, this means that the user will feel the difference in parameters on top of the desired parameters as shown in Equation (19).

B. Experimental Validation of Mass Identification Procedure

The procedure has been validated experimentally. The robot used for these experiments is shown in Figure 1a. This robot is equipped with wheel encoders to measure its movements. Each omni-directional wheel is capable of delivering a maximum of $103N$ of force in its longitudinal direction. The previously discussed procedure has been executed several times on the original robot without any modifications to it. The estimated mass and inertia of each experiment is shown in Table II. As can be seen from these Tables, the estimates are lower than the actual mass and inertia which are 36.1 kg and 0.73 kgm^2 respectively, meaning the procedure works as intended.

VIII. Experimental Validation

Experiments have been conducted to validate the combination of the disturbance observer with compliant control. The nominal parameters used are given in Table III and the desired compliant parameters are given in Table IV. The filter Q is chosen as a 1 Hz low-pass filter.

In order to check if the compliant control performs as expected, the same identification procedures used for the initial estimations is used. For the coulomb friction and viscous damping this means observing the force applied while following a constant velocity reference and repeating this for several velocities. For the mass and moment of inertia the force required to achieve a constant acceleration is used.

Axis	Nominal Mass/Inertia	Nominal Damping	Nominal Friction
x	33 kg	1.3795 Ns/m	26.3055 N
y	33 kg	0.7479 Ns/m	25.7372 N
θ	0.669 kgm^2	0.0955 Ns	4.6126 Nm

TABLE III: Nominal system parameters

Axis	Desired Mass/Inertia	Desired Damping	Desired Friction
x	18 kg	1.5 Ns/m	5 N
y	18 kg	1.5 Ns/m	5 N
θ	0.3 kgm^2	0.05 Ns	0.9 Nm

TABLE IV: Desired compliant parameters

More detail on these procedures can be found in Appendix A. If the nominal parameters are identical to the real parameters, the expected compliant parameters would be equal to the desired parameters. However, for stability reasons, the nominal parameters are chosen at the lower confidence bounds given in Table I such that for 95% confidence the nominal parameters are lower than the 'real' parameters. This results in the expected compliant parameters also depending on the difference between the 'real' and nominal parameters. Under the assumption that the system is in steady state, meaning $Q(s) = 1$, the expected compliant parameters can be calculated as following:

$$\begin{aligned} M_{\mathrm{e}} &= M_{\mathrm{d}} + (M_{\mathrm{r}} - M_{\mathrm{n}}) \\ D_{\mathrm{e}} &= D_{\mathrm{d}} + (D_{\mathrm{r}} - D_{\mathrm{n}}) \\ F_{\mathrm{c,e}} &= F_{\mathrm{c,d}} + (F_{\mathrm{c,r}} - F_{\mathrm{c,n}}), \end{aligned} \tag{28}$$

where the subscript $*_{\mathrm{e}}$ indicates that it is an expected parameter and F_{c} is the coulomb friction. The results of the experiments for the viscous damping and coulomb friction are shown in Figures 11, 12 and 13. The green lines in these Figures indicate the bounds in which the force is to be expected. These upper and lower bounds are based on the upper and lower confidence bounds given in Table I. As can be seen from the Figures, almost all measurement points lie within the bounds, meaning the compliant control performs as expected. Only at very low velocities the compliant force falls outside the bounds. This can possibly be explained by the fact that in that velocity region the used friction model is not accurate anymore due to the transition from coulomb friction towards static friction. The results of the compliant mass and inertia

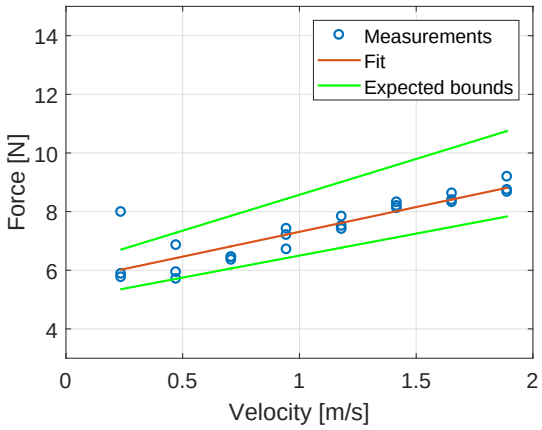

Fig. 11: Force required for a constant velocity in the x-axis is shown in blue. A fit through this data is shown by the red line and the expected bounds are shown by the green lines.

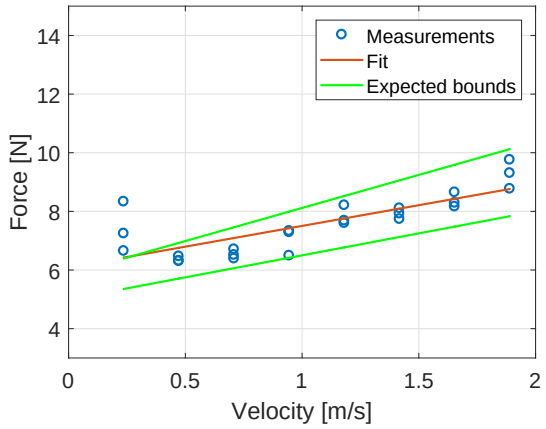

Fig. 12: Force required for a constant velocity in the y-axis is shown in blue. A fit through this data is shown by the red line and the expected bounds are shown by the green lines.

experiments are given in Table V. The bounds are based on the confidence bounds given in Table I. The results in Table V show that the expected mass and inertia lie within the bounds of the measured effective mass and inertia, meaning the compliant control performs as expected. These experiments show that the compliant control works for each axis independently, however certain issues arise when compliant control is active on multiple axis at the same time due to unmodeled interaction. During certain movements, uneven friction in the omni-wheels can create a net torque, which causes the robot to rotate. The cause of this rotation is not included in the nominal model, meaning the disturbance observer sees this as a user input and thus the compliant control will react to this incorrect observation. In certain scenarios this can lead to instability of the system.

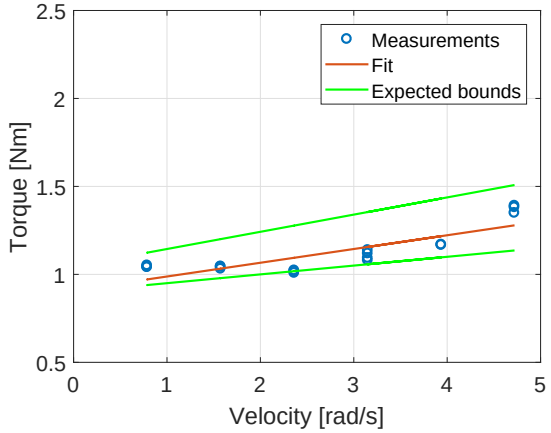

Fig. 13: Torque required for a constant rotational velocity in the θ-axis is shown in blue. A fit through this data is shown by the red line and the expected bounds are shown by the green lines.

	Mass (kg)	Inertia (kgm^2)
Lower bound estimate	18.71	0.325
Expected	21.5	0.360
Upper bound estimate	22.78	0.464

TABLE V: Expected compliant mass and inertia with estimated upper and lower bounds.

IX. Safety Features

Since the ropod will be interacting with people, maintaining safety is a very important aspect. That is why several safety features have been implemented. For the following features, no stability analysis is performed, so no theoretical guarantees can be given on the effects of these features on the system. However both features will only gradually reduce the amount of aid by the compliant control, so intuitively seen, this should not be able to cause instability. The following features have also been tested experimentally to check the stability and to subjectively evaluate by feeling the effect of these features during human-robot interaction.

A. Maximum Velocity

It is possible to set a maximum velocity $\dot{x}_{\text{max,l}}$ to which the ropod will aid the user. At higher velocities the ropod will offer reduced help and at velocities above $\dot{x}_{\text{max,u}}$ the ropod will not help the user at all. This way the ropod is not responsible for any potential damage caused by moving at high velocities, but at the same time, not restricting these higher velocities. This is achieved by changing the desired parameters $M_{\text{d}}, D_{\text{d}}$ and $F_{\text{c,d}}$ as a function of velocity towards the nominal parameters $M_{\text{n}}, D_{\text{n}}$ and $F_{\text{c,n}}$. A half cosine wave as function of velocity is used in the region between $\dot{x}_{\text{max,l}}$ and $\dot{x}_{\text{max,u}}$ to gradually shift the desired parameters to the nominal parameters. The effect of this change on the behavior of the robot is visible from the simplified dynamics from Equation (19). During this shift of the desired parameters, the effective parameters will shift towards the 'real' parameters, meaning the aid by the compliant control will decrease. At the velocity $\dot{x}_{\text{max,u}}$ where the desired parameters are equal to the nominal parameters, the dynamics are equal to the original dynamics without compliant control. This can also be visualized from Figure 6 where all the impedance gains will go to zero when the desired parameters are equal to the nominal parameters.

B. Maximum Acceleration

The second safety feature is to limit the acceleration up to which the robot helps the user. Accelerating faster than this limit is still possible, however this additional force has to be provided entirely by the user. This is achieved by saturating the measured acceleration which is used by the disturbance observer. This way if the user decides to accelerate faster than the limit, the observer will not observe this increase in force and thus the compliant control will not assist the user more than it already did.

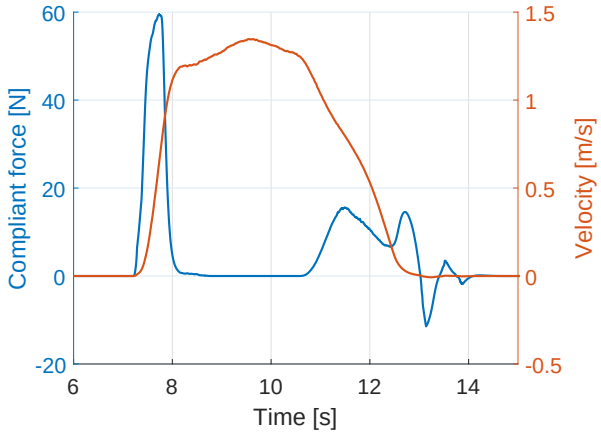

Fig. 14: Compliant aided force with the maximum velocity safety feature enabled.

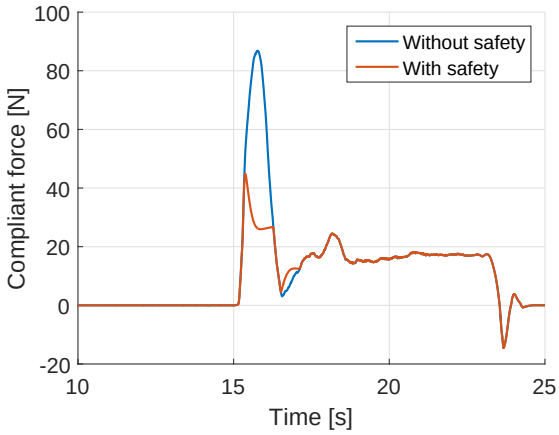

Fig. 15: Compliant aided force with the maximum acceleration safety feature enabled.

C. Experimental Validation

Both safety features have been verified experimentally. The maximum velocity safety feature has been tested by setting $\dot{x}_{\text{max,l}}$ equal to 0.75 m/s and $\dot{x}_{\text{max,u}}$ to 1.25 m/s. During the experiment the robot was pushed manually to a speed of roughly 1.3 m/s. The result of this experiment is shown in Figure 14. As can be seen from this Figure, at a velocity of 0.75 m/s the effort by the compliant control starts getting reduced and at a velocities of 1.25 m/s and higher, the compliant control is completely turned off. When the velocity goes below 1.25 m/s the compliant control starts helping again. During the experiments it was noticed that with this safety feature the user is really discouraged to go above the velocity limit, since then the aid will be reduced. However the system is not prohibiting the user to go above the maximum velocity. This can also be seen from the velocity profile. Initially the robot accelerates quickly since it aids the user, but when the velocity limit is reached the user has to apply all the force, resulting in the lowered acceleration. The maximum acceleration safety feature has been tested by setting the acceleration limit to 0.5 m/s^2 and then pushing the robot abruptly with a lot of force, followed by a constant velocity motion. The red line in Figure 15 shows the force the compliant control applied during this experiment and the blue line shows the force it would have applied if the safety feature would be disabled. As can be seen in the beginning during the initial push, the control action is limited by the safety feature, but during constant velocity the aid is not affected by the safety feature. This prevents the robot from slipping during high interaction forces. Just after the initial peak a second region can be identified which shows the control action is limited. In this case, the user wanted to decelerate too quickly and therefore this force was limited.

X. Conclusions and Future Work

The first objective of this research was to develop a compliant control strategy which allows a wheeled mobile robot to interact with people and the environment in a compliant way without the use of force sensors. To achieve this, three different active compliant control strategies have been selected to be further investigated. In order to get a force estimate of the user input which is required for the compliant control strategies, a disturbance observer has been developed which uses a dynamical model of the system. The disturbance observer has been coupled to the compliant control to achieve the desired objective. For this combination, performance analyses have been performed in order to compare the suitability of each compliant control algorithm. Design guidelines are presented for each combination of compliant control with the disturbance observer. Impedance control was selected due to the higher amount of customizability over the force feedback method and better performance compared to admittance control. In order to handle variations in mass and inertia while preserving stability and performance, a procedure has been developed which is capable of quickly estimating the mass and inertia of the robot plus load. This procedure is guaranteed to slightly underestimate these parameters, which is essential for the stability of the system. The performance analysis revealed that any discrepancy in this estimation will be added to the dynamics felt by the user. The performance and stability of the combination of the compliant control with the disturbance observer has been verified experimentally. The experiments show that the proposed method is capable of changing the mass/inertia, viscous damping and coulomb friction a user experiences. This works for each axis individually, however due to unmodeled interaction between the xy axis and the θ axis, the system can become unstable if all three axes have compliant control activated at the same time. This issue is not present when compliant control is active in only the xy direction. Lastly, two safety features have been developed and experimentally tested which limit the aid at high velocities and limits the forces during high acceleration to prevent wheel slip.

For future work, the ability to take kinematic constraints

imposed by the load could be added. Several loads which are intended to work with this system have several fixed wheels, meaning that motion in certain directions is no longer possible. If these kinematic constraints are known beforehand, it would be possible to incorporate this in the disturbance observer and impedance control. The robot used in this research uses omni-wheels, however the final ropod will feature caster wheels. The initial orientation of these caster wheels can have a large impact on the friction acting on the system, meaning that the current friction model would no longer be sufficient. Another interesting topic for future work is to look at a strategy which is capable of detecting the users force while the robot is not moving. The current implementation uses the wheel encoders as input and is thus not capable of observing and replying to forces when the robot is not in motion. This means the user has to overcome the robots static friction themselves before the compliant control starts to help. Another feature which could be added is the capability to detect when the robot is standing on a sloped surface. Currently gravity is not yet incorporated in the model of the disturbance observer and thus gravity will be treated as an external user input and respond to it, which is undesirable.

REFERENCES

[1] Seegrid, "Automated Guided Vechicles: The Hot Trend In Distribution Centers," *http://www.roboticstomorrow.com/content.php?post_type=1892*.

[2] "Ultra-flat, ultra-flexible, cost-effective robotic pods for handling legacy in logistics," *http://cordis.europa.eu/project/rcn/206247_en.html*.

[3] M. Florek-Jasinska, T. Wimbock, and C. Ott, "Humanoid compliant whole arm dexterous manipulation: Control design and experiments," *IEEE International Conference on Intelligent Robots and Systems*, no. Iros, pp. 1616–1621, 2014.

[4] A. Jain and C. C. Kemp, "Pulling open doors and drawers: Coordinating an omni-directional base and a compliant arm with equilibrium point control," *Proceedings - IEEE International Conference on Robotics and Automation*, pp. 1807–1814, 2010.

[5] F. Ficuciello and L. Villani, "Compliant hand-arm control with soft fingers and force sensing for human-robot interaction," *Proceedings of the IEEE RAS and EMBS International Conference on Biomedical Robotics and Biomechatronics*, pp. 1961–1966, 2012.

[6] J. Frémy, F. Ferland, M. Lauria, and F. Michaud, "Force-guidance of a compliant omnidirectional non-holonomic platform," *Robotics and Autonomous Systems*, vol. 62, no. 4, pp. 579–590, 2014.

[7] K. S. Kim, A. S. Kwok, G. C. Thomas, and L. Sentis, "Fully omnidirectional compliance in mobile robots via drive-torque sensor feedback," *IEEE International Conference on Intelligent Robots and Systems*, no. Iros, pp. 4757–4763, 2014.

[8] A. Dietrich, T. Wimböck, and A. Albu-Schäffer, "Dynamic Whole-Body Mobile Manipulation with a Torque Controlled Humanoid Robot via Impedance Control Laws, 2011.pdf," pp. 3199–3206, 2011.

[9] S. Haddadin, A. Albu-Schäffer, A. De Luca, and G. Hirzinger, "Collision detection and reaction: A contribution to safe physical human-robot interaction," *2008 IEEE/RSJ International Conference on Intelligent Robots and Systems, IROS*, pp. 3356–3363, 2008.

[10] A. De Luca and R. Mattone, "Sensorless robot collision detection and hybrid force/motion control," *Proceedings - IEEE International Conference on Robotics and Automation*, vol. 2005, no. April, pp. 999–1004, 2005.

[11] K.-t. Song, Y.-c. Liao, and Y.-l. Jian, "Sensorless Assistive Torque Design for a Lower Extremity Exoskeleton," *International Conference on Control, Automation and Systems (ICCAS 2014)*, vol. 14, no. Iccas, pp. 793–797, 2014.

[12] S. Katsura and K. Ohnishi, "Human Cooperative Wheelchair for Haptic Interaction Based on Dual Compliance Control," *IEEE Transactions on Industrial Electronics*, vol. 51, no. 1, pp. 221–228, 2004.

[13] B. J. Mohler, W. B. Thompson, S. H. Creem-Regehr, H. L. Pick, and W. H. Warren, "Visual flow influences gait transition speed and preferred walking speed," *Experimental Brain Research*, vol. 181, no. 2, pp. 221–228, 2007.

[14] B. Siciliano and O. Khatib, *Handbook of Robotics*. Springer Publishing, 2008.

[15] C. Ott, R. Mukherjee, and Y. Nakamura, "A Hybrid System Framework for Unified Impedance and Admittance Control," *Journal of Intelligent and Robotic Systems: Theory and Applications*, vol. 78, no. 3-4, pp. 359–375, 2014.

[16] S. Inagaki, T. Suzuki, and T. Ito, "Design of man-machine cooperative nonholonomic two-wheeled vehicle based on impedance control and time-state control," *Proceedings - IEEE International Conference on Robotics and Automation*, pp. 3768–3773, 2009.

[17] K. Irie, S. Katsura, and K. Ohishi, "Wideband Motion Control by Acceleration Disturbance Observer," in *2006 12th International Power Electronics and Motion Control Conference*, pp. 361–366, IEEE, aug 2006.

[18] E. Sariyildiz and K. Ohnishi, "A Guide to design disturbance observer," *Journal of Dynamic Systems, Measurement, and Control*, vol. 136, no. 2, p. 021011, 2013.

[19] F. Boeren, T. Oomen, and M. Steinbuch, "Iterative motion feedforward tuning: A data-driven approach based on instrumental variable identification," *Control Engineering Practice*, vol. 37, pp. 11–19, 2015.

[20] D. Rijlaarsdam, P. Nuij, J. Schoukens, and M. Steinbuch, "Frequency Domain Based Friction Compensation - Industrial Application to Transmission Electron Microscopes -," *Proceedings of the American Control Conference*, pp. 4093–4098, 2011.

[21] I. Polat, "A note on passivity based stability conditions for bilateral teleoperation," *IFAC Proceedings Volumes (IFAC-PapersOnline)*, vol. 18, no. PART 1, pp. 320–325, 2011.

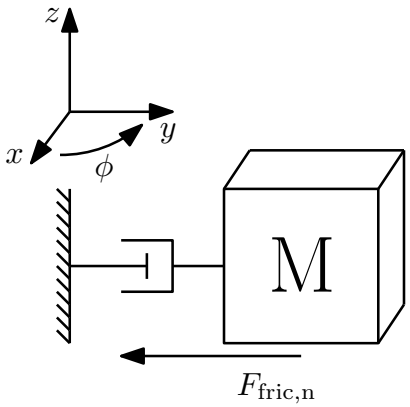

Fig. 16: Schematic representation of the used dynamic model

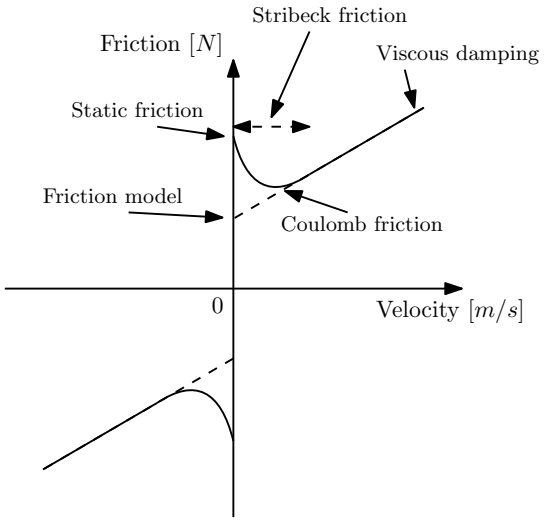

Fig. 17: Friction model

APPENDIX A
INITIAL PARAMETER ESTIMATION

A. Dynamic Model

The degrees of freedom of this robot consist of two translational axes and one rotational axis. Since the robot uses omni-directional wheels, the two transnational and single rotational axis can be decoupled and such they can be considered as three independent single degree-of-freedom systems. Each degree of freedom is simplified for modeling purposes to a mass-damper system with friction. A schematic drawing of this model is given in Figure 16.

The two translations are movements over the x and y axis in [m] while the rotational movement is around the z axis, called the ϕ direction in [rad].

B. Friction Model

In the dynamic model equations given by (1) there is the friction term $F_{\text{fric,n}}$. One commonly used model to describe the friction of a system is called the Stribeck curve. This curve describes the relationship between the velocity of an object and the friction force acting on it. A typical Stribeck curve is shown in Figure 17.

The friction $F_{\text{fric,n}}$ is modeled as a simplified version of this Stribeck curve where the static friction and the coulomb friction are equal. This results in the following expression for $F_{\text{fric,n}} = F_{c,n}\text{sign}(\dot{x})$ where $F_{c,n}$ represents the friction force at zero velocity. This is visually shown in Figure 17 as the dashed line. This simplification only holds when the Stribeck friction area is relatively small compared to the typical operating velocity. In Section A-C the friction as a function of velocity will be determined. The viscous damping shown in Figure 17 is represented by the term $D_{\text{n}}\dot{x}$ in (1).

C. Parameter Identification

For the dynamic model described in (1) the mass, damping and friction of the robot are required. These values have been determined experimentally for all three axes individually. In order to determine the damping and friction the following experiments have been conducted. A reference trajectory is given to the robot. This position reference is followed by an existing position controller in the TURTLE. The position reference consists of three parts: a constant acceleration until a desired velocity is reached, a constant velocity part and a constant deceleration to standstill. An example of such a reference is shown in Figure 18.

During the constant velocity part of the reference, only two types of forces act on the robot; the coulomb friction and the viscous damping. As mentioned earlier, the coulomb friction has no proportional scaling with velocity while the damping does have proportional scaling with velocity. This means that both parameters can be identified when repeating this experiment for at least two different constant velocities and observing the forces applied to maintain the constant velocity. Due to the presence of noise and other effects, repeating the experiment for a range of velocities will increase the accuracy of the estimation. This experiment has been conducted for all three axes with several different constant velocity references. The results of these experiments are shown in Figures 19, 20 and 21.

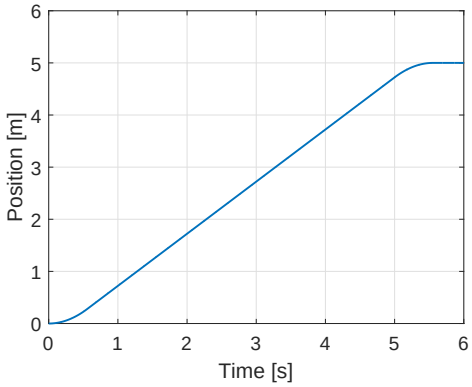

Fig. 18: Reference trajectory with a constant velocity of 1 m/s and acceleration of 1.8 m/s^2

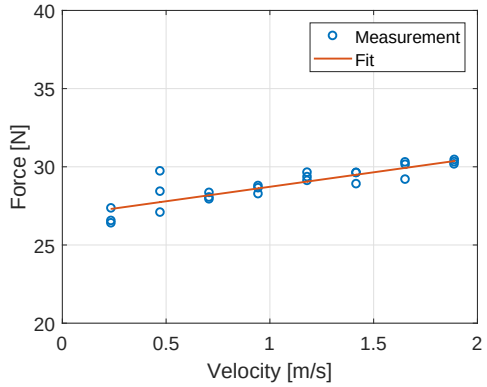

Fig. 19: Applied force and fit for a constant velocity in the x direction

The data shows that the force scales relatively linear with velocity. The blue fit through the data is a linear fit from which the viscous damping and coulomb friction can be estimated. The damping is equal to the slope of the fit while the coulomb friction is equal to the offset of the fit at velocity $\dot{x} = 0\ m/s$. The parameter estimations plus their 95% confidence bounds are given in Table I. The mass of the robot has been weighed using a weighing scale. The moment of inertia is estimated using a different procedure. A reference with constant acceleration is given to the rotation controller of the robot. The torque required to follow this reference is reduced by the coulomb friction torque and the viscous damping torque estimated before, such that the resulting torque is only caused by acceleration of the mass. The average of this torque required is then divided by the average acceleration to obtain the robot's moment of inertia.

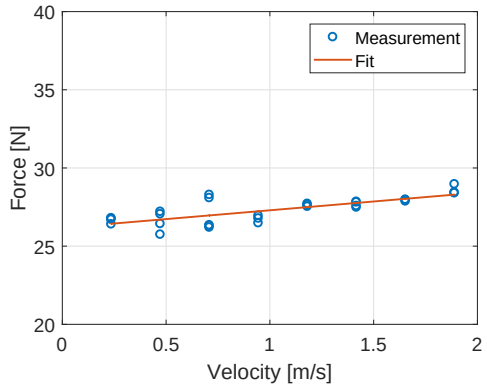

Fig. 20: Applied force and fit for a constant velocity in the y direction

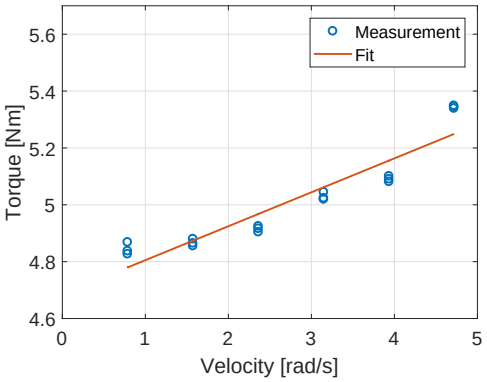

Fig. 21: Applied force and fit for a constant velocity in the ϕ direction

APPENDIX B
STABILITY WITH FRICTION

The stability of a linear time invariant system with friction and friction compensation by the compliant control can be proven with the use of passivity theory [21]. The overall system can be split into two systems which are connected to each other. The first system is the linear system which is discussed in Section VI and the second system is the non-linear friction, friction observer and friction compensation. The connection between these two systems is stable if both systems are stable and both systems are passive. The stability of the linear system has already been discussed in Section VI. A stable linear time invariant system is passive if the following holds

$$\mathrm{Re}\{G(i\omega)\} > 0 \qquad \text{for all } \omega \in \mathbb{R} \cup \{\infty\}. \tag{29}$$

In this Equation, the transfer-function G is the transfer-function between the input and output of the system of which passivity should be proven. In the case of the friction analysis, the input is the velocity of the robot and the output the force generated by all friction blocks combined. This way if the friction system is passive and the system on which this friction works is passive, the combination of both is stable.

A. Impedance Control

For impedance control combined with the disturbance observer the input-output situation is shown in Figure 22. In this Figure, F_{sys} contains the real friction of the system $F_{\text{fric,r}}$, the compensation of the nominal friction by the impedance control $F_{\text{fric,n}}$ and the addition of the desired friction $F_{\text{fric,d}}$ by the impedance control as well. This can be modeled as

$$F_{\text{fric}} = \text{sign}\left(\dot{x}\right)\left(-F_{\text{fric,r}} + F_{\text{fric,n}} - F_{\text{fric,d}}\right) \tag{30}$$

which is passive as long as $-F_{\text{fric,r}} + F_{\text{fric,n}} - F_{\text{fric,d}} < 0$, meaning energy will always be dissipated. The total system is stable if the system shown in Figure 22 and Equation (30) both are passive. The transfer-function between $\dot{x}$ and F_{fric} under the assumption $Q(s) \approx 1$ is given by

$$\frac{\dot{x}}{F_{\text{fric}}} = \frac{1}{D_{\text{r}} - D_{\text{n}} + D_{\text{d}} + M_{\text{d}}s - M_{\text{n}}s + M_{\text{r}}s} \tag{31}$$

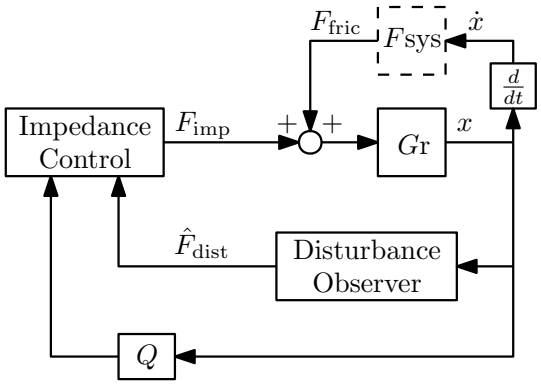

Fig. 22: Friction input-output for disturbance observer combined with impedance control

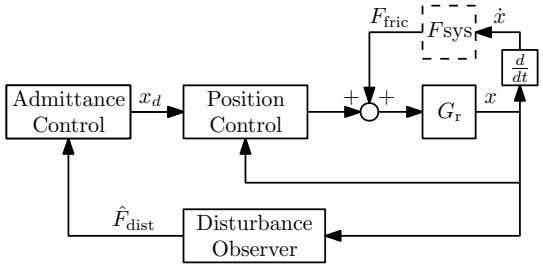

Fig. 23: Friction input-output for disturbance observer combined with admittance control

which can be rewritten into

$$\frac{\dot{x}}{F_{\text{fric}}} = \frac{\left(D_{\text{r}} - D_{\text{n}} + D_{\text{d}}\right) - \left(M_{\text{d}} - M_{\text{n}} + M_{\text{r}}\right) jw}{\left(D_{\text{r}} - D_{\text{n}} + D_{\text{d}}\right)^2 + \left(M_{\text{d}} - M_{\text{n}} + M_{\text{r}}\right)^2 \omega^2}. \tag{32}$$

The system is considered passive if (29) holds, meaning

$$\frac{\dot{x}}{F_{\text{fric}}} = \frac{\left(D_{\text{r}} - D_{\text{n}} + D_{\text{d}}\right)}{\left(D_{\text{r}} - D_{\text{n}} + D_{\text{d}}\right)^2 + \left(M_{\text{d}} - M_{\text{n}} + M_{\text{r}}\right)^2 \omega^2} > 0 \qquad \text{for all } \omega \in \mathbb{R} \cup \{\infty\}. \tag{33}$$

Therefore $D_{\text{r}} - D_{\text{n}} + D_{\text{d}}$ should be larger than 0 for the system to be passive. This results in two criteria required for the total system with friction to be stable:

$$\begin{aligned} -F_{\text{fric,r}} + F_{\text{fric,n}} - F_{\text{fric,d}} &< 0 \\ D_{\text{r}} - D_{\text{n}} + D_{\text{d}} &> 0 \end{aligned} \tag{34}$$

together with the criteria presented in VI-A. These criteria do not guarantee absolute stability since the assumption $Q(s) \approx 1$ was made, however they do act as guidelines, which in practice have shown to be effective.

B. Admittance Control

The same theory can be applied to admittance control. The input-output relation for the friction is shown in Figure 23. In this Figure, F_{sys} is equal to (30). Under the assumption of a perfect position controller and $Q(s) \approx 1$, the input-output relationship is also equal to (31). This means both passivity and stability criteria are equal to (34) and those found in VI-B.

C. Force Feedback

For the force feedback algorithm the input-output relationship for the friction is shown in Figure 24. The system F_{sys} can be written as

$$F_{\text{fric}} = \text{sign}\left(\dot{x}\right)\left(-F_{\text{fric,r}} + KF_{\text{fric,n}} - KF_{\text{fric,r}}\right) \tag{35}$$

and the input-output transfer-function for $Q(s) \approx 1$ as

$$\frac{\dot{x}}{F_{\text{fric}}} = \frac{K+1}{D_{\text{comp}} + M_{\text{comp}}s} \tag{36}$$

with:

$$\begin{aligned} D_{\text{comp}} &= D_{\text{r}} - \left(D_{\text{n}} + D_{\text{r}}\right)K \\ M_{\text{comp}} &= M_{\text{r}} - \left(M_{\text{n}} + M_{\text{r}}\right)K. \end{aligned} \tag{37}$$

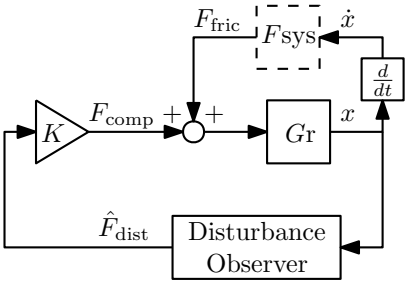

Fig. 24: Friction input-output for disturbance observer combined with force feedback control

This can be rewritten into

$$\frac{\dot{x}}{F_{\text{fric}}} = \frac{(K+1)\,(D_{\text{comp}} - M_{\text{comp}} j\omega)}{D_{\text{comp}}^2 + M_{\text{comp}}^2 \omega^2}, \tag{38}$$

meaning the system is passive if

$$\begin{aligned} \frac{\dot{x}}{F_{\text{fric}}} = \frac{(K+1)\,D_{\text{comp}}}{D_{\text{comp}}^2 + M_{\text{comp}}^2 \omega^2} > 0 \\ \text{for all } \omega \in \mathbb{R} \cup \{\infty\}. \end{aligned} \tag{39}$$

Assuming $K > 0$, both systems are passive and thus the interconnection is stable if:

$$\begin{aligned} -F_{\text{fric,r}} + K F_{\text{fric,n}} - K F_{\text{fric,r}} < 0 \\ D_{\text{r}} - (D_{\text{n}} + D_{\text{r}})\, K > 0 \end{aligned} \tag{40}$$

in addition to the stability criteria found in VI-C.